A New Hybrid Pore-Scale Simulation Method to Characterize Nanoparticles Transport and Attachment Behaviors

Yue Li[1], Bin Yuan[1], Can Ke[1], Xvpeng Liu[1], Mingliang Han[1], and Huilin Hou[1]

[1]China University of Petroleum East China - Qingdao Campus

January 3, 2023

Abstract

A hybrid pore-scale simulation method using Lattice-Boltzmann (LB) coupled with Langevin-Dynamics (LD) is proposed to investigate the transport physics of nanoparticles in microchannel. The controlling factors (i.e., ionic strength, particle diameter and Reynolds number) are investigated in the attachment process of NPs. It is observed that a threshold value of attachment efficiency exists as the ionic strength increases to about 0.01 M. Moreover, the ionic strength of aqueous phase has critical effect on the transport behavior of NPs. For the purpose of quantitatively characterizing the structure of NP suspensions under varying conditions, a general phase diagram including three flow patterns (isolated, transitional and clustered regime) is first proposed for NP suspension with specified ionic strength and Reynolds number. The outcomes of this work provide valuable insight on the critical importance of the particle size, ionic strength and hydrodynamic effects on the attachment and transport process of NPs in porous media

A New Hybrid Pore-Scale Simulation Method to Characterize Nanoparticles Transport and Attachment Behaviors

Yue Li[1], Bin Yuan[1,2*],Can Ke[1], Xvpeng Liu[1], Mingliang Han[1], Huilin Hou[1]

1. School of Petroleum Engineering, China University of Petroleum (East China), Qingdao 266580, P. R. China

2. Key Laboratory of Unconventional Oil & Gas Development (China University of Petroleum (East China)), Ministry of Education, Qingdao 266580, P. R. China

Corresponding author: yuanbin@upc.edu.cn

Abstract

A hybrid pore-scale simulation method using Lattice-Boltzmann (LB) coupled with Langevin-Dynamics (LD) is proposed to investigate the transport physics of nanoparticles in microchannel. The controlling factors (i.e., ionic strength, particle diameter and Reynolds number) are investigated in the attachment process of NPs. It is observed that a threshold value of attachment efficiency exists as the ionic strength increases to about 0.01 M. Moreover, the ionic strength of aqueous phase has critical effect on the transport behavior of NPs. For the purpose of quantitatively characterizing the structure of NP suspensions under varying conditions, a general phase diagram including three flow patterns (isolated, transitional and clustered regime) is first proposed for NP suspension with specified ionic strength and Reynolds number. The outcomes of this work provide valuable insight on the critical importance of the particle size, ionic strength and hydrodynamic effects on the attachment and transport process of NPs in porous media.

1 INTRODUCTION

Nanoparticles (NPs) have been extensively applied in various fields with distinctive size-dependent properties: relatively large surface area and self-assembly behavior[1,2]. In solar thermal fields, NPs are great material for enhancing the performance of solar systems as their high thermal conductivity[3]. In biomedical and pharmaceutical fields, NPs, as a better drug carrier, could increase the therapeutic efficiency of the drugs, weaken side effects and improve patient compliance[4]. In electronics fields, NPs are good sensors and photonic materials for their unique structural, optical and electrical properties[5]. In mechanical industries, NPs are also very promising for coating, lubricants and adhesive applications[6]. In the petroleum industry, NPs have a variety of applications[7]. Nano-enhanced drilling fluid could form high-quality mud cake, improve wellbore stability during the drilling process[8]. NPs also play an important role in enhancing oil recovery especially in tertiary oil recovery: stabilizers of emulsion and foam[7], rock wettability alteration[9], interfacial tension reduction[9].

In the above process, one of the emergent concerns in common is to quantitatively characterize the transport and attachment of nanoparticles in pore scale. Various methods have been developed to investigate it in the last few decades. The Random sequential adsorption (RSA) is one of the earliest models to simulate particles[10,11]. While to model a typical adsorption process, several strong assumptions have to be followed: all particles adsorb directly on the surface, external forces, hydrodynamics and diffusion are negligible[10,11]. Subsequently, Eulerian-Eulerian (EE) and Eulerian-Lagrangian (EL) are modeling methods that have been introduced to investigate particles transport and attachment processes[12,13]. In EE models, the base fluid and particles are continuous phases. Therefore, EE models are suitable for dense particles concentration which particles could be considered a continuous phase[14]. However, EE models cannot investigate the behavior of particles such as clustering[15]. In EL models, the base fluid is described by the Eulerian approach and NPs are simulated by a Lagrangian approach which could be used for tracking the trajectory of particles. The Euler-Lagrange model was developed for simulating fine particle suspension in liquids: sedimentation, particle-induced stratification, and particle-laden turbulence[16-18]. Additionally, the Euler-Lagrange model was used to investigate the influence of Brownian and gravitational forces on the velocity and transport of induced CuO NPs in oil phase [19]. While with the increased of injecting particle number, tracking trajectory of every particle becomes intractable[15].

The above works cannot take account of the effects of ion in solution. While the ionic strength affects the structure of NP suspension. Brownian dynamics was applied to investigate the aggregation process of TiO_2 NPs in aqueous suspensions, the increased ionic strength would contribute the aggregation rate of NPs[20]. A DEM-based model was developed for simulation of aggregation in suspensions of α-alumina NPs[21].The aggregation structures were captured with different PH, solid volume fraction and AC electric fields. A constant-number direct simulation Monte Carlo (DSMC) model was developed for analysis of NP agglomeration in aqueous suspensions. The result is still the ionic strength strongly influencing the aggregation process of NPs[22]. The Lattice Boltzmann-Smoothed Profile method was used to investigate ionic strength and zeta potential effects on colloid transport and retention processes. The result showed the increase of ionic resulted in larger agglomerates, decreasing of pore void fraction and hydraulic conductivity[23]. In addition, some experiment results showed the distribution pattern of NPs could not be only in aggregation structures, but also in ordered pattern with various ionic strength[24-26]. While the investigation of distribution pattern is focused on quiescent state. How to simulate the experiment result qualitatively and quantitatively seems challenging. There are less researches on the flow pattern of NPs in the transport process with different ionic strength, which hinders the understanding of underlying mechanisms of NPs transport in porous media.

In this work, we adopt and extend a two-way coupled lattice Boltzmann-Langevin dynamics (LB-LD) method developed by Liu et al.[27-29] to investigate the transport and attachment of charged NPs in a microchannel. LB is a highly scalable method that can simulate single-phase and multiphase fluid flows and for incorporating additional physical complexities [30,31]. As previous demonstrated[27], LD when properly coupled with the LB method could simulate nanoscale particle and polymer suspensions in the presence of both thermal fluctuation and long-range many-body hydrodynamic interactions with good accuracy. This study investigates the

transport and attachment of hundreds of charged NPs in a microchannel, mainly focusing on the effect of ionic strength and hydrodynamic effect on the transport and attachment processes.

The body of this work is organized as follows, the details of the lattice Boltzmann method and Langevin dynamics are described in Section 2. Validations are presented in Section 3. Results and discussion are presented in Section 4, followed by the conclusions in Section 5.

2 THEORY AND METHOD

2.1 Langevin dynamics method

The motion of NPs could be described by Langevin dynamics. Figure 1 shows the force analysis of the NP in aqueous phase.

Where m_p^i is the mass of NP i ,$\overrightarrow{S}^i{}_P$ is the random force of NPs reflecting the thermal fluctuation effect of fluid,$\overrightarrow{F}^i{}_P$ is the friction force of NPs i ,$\overrightarrow{V}^i{}_P$ is the van der Waals force of NPsi , $\overrightarrow{E}^i{}_P$ the electrostatic force of NPs i. For the calculation of $\overrightarrow{V}^i{}_P$, it can be divided into the van der Waals force between NPs and the van der Waals force between NPs and the microchannel surface. The van der Waals force between NPs can be calculated through the following equation[32]:

Where Acc is the Hamaker constant, N is the total number of NPs, W ($\overrightarrow{D}_{\mathrm{ij}}$) is the van der Waals potential energy between active NPs, T is the absolute temperature,D_{ij} is the minimum distance of NP i and NPj , R_i and R_j is the radius of NP i and NP j .

The van der Waals force between NPs and microchannel surface can be calculated as follows

Where R is the radius of the NP, $\overrightarrow{D}$ is the minimum distance between NP surface and microchannel surface.

The calculation of $\overrightarrow{E}^i{}_P$ can be divided into electrostatic force between NPs and electrostatic force between NPs and microchannel surface. The electrostatic force between NPs can be calculated by the following equation.

Where κ is reciprocal of Debye length, Z is the interaction constant. Z can be calculated by Formulas.

Where ε_0 is the vacuum dielectric constant,ε is the relative dielectric constant of water, $z$is the electrolyte valence and φ_1 is the surface potential of NP.

The electrostatic force between NPs and microchannel surface can be calculated by the following equation

For the friction force of NPs in the fluid, it is linearly correlated with the relative velocity of NPs and the viscous fluid around them, which can be calculated by Formulas.

Where the friction coefficient ζ can be obtained by the Stokes formula:$\zeta = 3\pi\mu_w d_p\psi$.

In the formula, μ_w is the dynamic viscosity of the aqueous phase, ψ is the shape coefficient of the NPs, and the value range between 0 to 1, where w is the aqueous phase, $d_p$is the particle diameter, the velocity of water$\overrightarrow{u}_w(\overrightarrow{r_P}, t)$ at the corresponding position of particles needs to be obtained through interpolation.

The Brownian motion of NPs due to instantaneous momentum fluctuations from solvent atoms can be characterized by random force, which satisfies the following relationship

where ?, ?[?]{x, y}, i and j run through all the particle indices, $?_{\mathrm{ij}}$ and $?_{??}$ are Kronecker deltas, ?(t-t') is the Dirac-delta function, $\mathrm{K_B}$ is the Boltzmann constant, T is the absolute temperature of the fluid bath, and the angle brackets denote the average over the ensemble of realizations of the random variables.

The velocity and displacement of NPs at corresponding time can be obtained by solving the above force

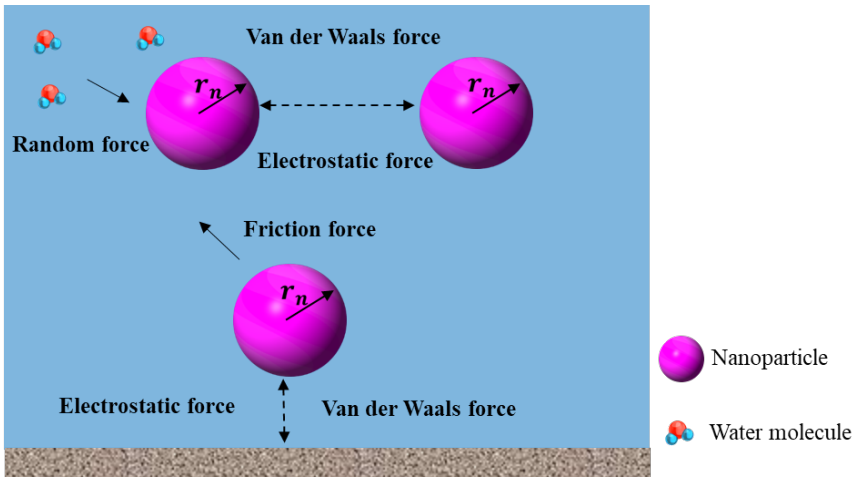

FIGURE 1 Schematic diagram of force analysis of NPs in aqueous phase

2.2 Lattice Boltzmann method

As a new alternative approach to solving the Navier-Stokes equations, LBM is used for simulate base fluid phase. LBM as a mesoscopic particle-based algorithm assumes the fluid flow is composed of a collection of pseudo-particles. LBM solves the discrete Boltzmann equation in velocity space by the particle propagation and collision processes over a discrete lattice mesh. Complex collisions could be simplified by the single-relaxation-time (SRT) Bhatnagar-Gross-Krook collision operator[33]. Multi-relaxation and entropy collision operators can also be used to gain high numerical stability[34-36]. The evolution of particle distribution function in single-relaxation-time is as follows.

τ is single relaxation time, $\overrightarrow{e}_i$is the unit vector of the particle velocity component andf_i is the particle distribution function in$i$ direction. f_i^s is the distribution function of the force source term of the fluid in the direction i . Δtand Δr is the time step and the lattice step, correspondingly. In the range from incompressible to slightly compressible ($Ma < 0.3$), the lattice Boltzmann equation can be restored to the Navier-Stokes equation, and the expression of the distribution function of the equilibrium state f_i^{eq}can be obtained

The fluid density ρ and velocity $\overrightarrow{u}$ could be derived as corresponding the zeroth and first order moments off_i .

Cs is pseudo sound velocity, ν is fluid dynamic viscosity, Q is defined as discrete direction number, ω_i is weight coefficient in i direction, $\overrightarrow{u}$is fluid velocity, I is characteristic tensor, initial value can be given according to the actual situation. The macroscopic properties of fluid such as pressure and velocity are obtained by calculating the distribution function.

2.3 LB-LD coupling method

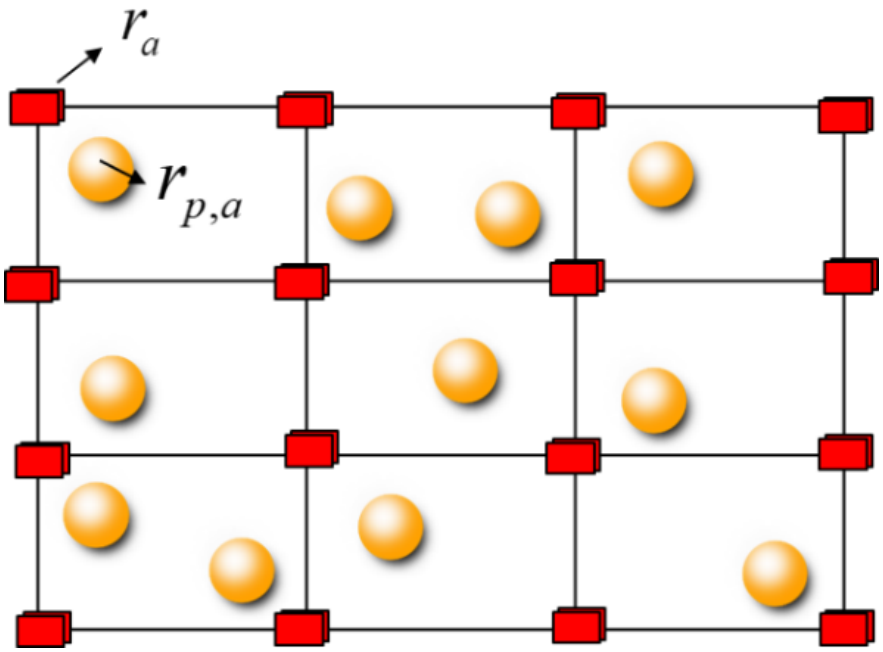

FIGURE 2 Schematic of NPs and fluid nodes

The coupling between the LB and the LD methods is based on the two-way coupling scheme originally proposed by Liu et al.[27,28]. Specifically, the hydrodynamic force $\overrightarrow{F}_P^W$ is defined as the total force acting on the fluid by NPs, and the formula is as follows

Where the fluid velocity at the NP position needs to be obtained by interpolation (Figure **2**).

Ahlrichs[37] uses bilinear interpolation to obtain the velocity of the fluid and reads only one layer of fluid nodes around the NPs, which is the first order accuracy. The weight function is expressed as follows

where, r_a represents the location of the fluid node and $r_{p,a}$ is the location of the center of the NPs.

Peskin[38] proposed a new format of the weight function to read the two-layer fluid nodes around the NPs, which is the second-order accuracy. The expression is as follows:

Following Liu et al.[27], this study utilizes the bilinear interpolation method based on spatial point distance to obtain the velocity of the fluid in the NP position, where the fluid velocity at the NP position can be obtained by interpolation

Here, N_l represents the number of fluid nodes in the lattice space occupied by NPs. To add hydrodynamic force to the fluid nodes, it is necessary to construct the format to meet the format and magnitude under the lattice Boltzmann condition.

First define impulse density [30]

At each time step, the pulse density assigned to the fluid node can be calculated by the above formula. At the same time, the pulse density can be transformed into the distribution function of the force source term by the scheme proposed by He et al.[39].

The force source term distribution function is introduced into the lattice Boltzmann evolution equation to simulate the interaction between NPs and fluid.

When using lattice Boltzmann method, the dimension of physical quantity needs lattice unit system. Therefore, the physical quantities involved in LB-LD need unit conversion in this simulation. In the lattice Boltzmann unit system, the lattice length, time step and fluid density are set to 1. The standardized single relaxation time and lattice Boltzmann viscosity are $\tau_{\mathrm{LB}} = \tau/\Delta t$ and$\upsilon_{\mathrm{LB}} = (2\tau_{\mathrm{LB}} - 1)/6$ respectively.

The conversion coefficient selected in this study: length conversion coefficient L_r is 50 nm, time conversion coefficient is $t_r = \upsilon_{\mathrm{LB}}\upsilon^{-1}L_r^2$, and density conversion coefficient is 1000 kg/m^3. The time conversion coefficient depends on the fluid dynamic viscosity and lattice Boltzmann relaxation time. The density of the fluid is set to 1.2 mPa·s. The absolute temperature is set to 373 K, for the sake of clarity, the LB correspondence of the previously introduced quantities in the physical unit is shown in the following label ' LB '. LB in this research is based on single relaxation BGK collision model. When using multi relaxation method[40], more parameters can be adjusted to obtain higher numerical stability, and the corresponding unit conversion is not the same.

3 MODEL VERIFICATION

Example 1: Single particle relaxation in viscous flow

In this case, we consider the deceleration process of a SiO_2 NP with momentum not zero in the static viscous flow field to verify the validity of the implementation of the LB-LD two-way coupling scheme[27]. Each LB boundary considers the periodic boundary, and sets two-dimensional computational domains of different sizes (50^2, 70^2, 100^2) to consider the influence of the flow field range on the deceleration process of a single NP. The mass of NPs under LB unit system was set to be 29.3 and there is an initial velocity in the X direction. The velocity was 0.01, and the initial position was set at the center of the calculation domain. The diameter of NPs was set to100 nm, and the friction coefficient is set to 0.48. Only the friction force between NPs and fluid is considered in this example.

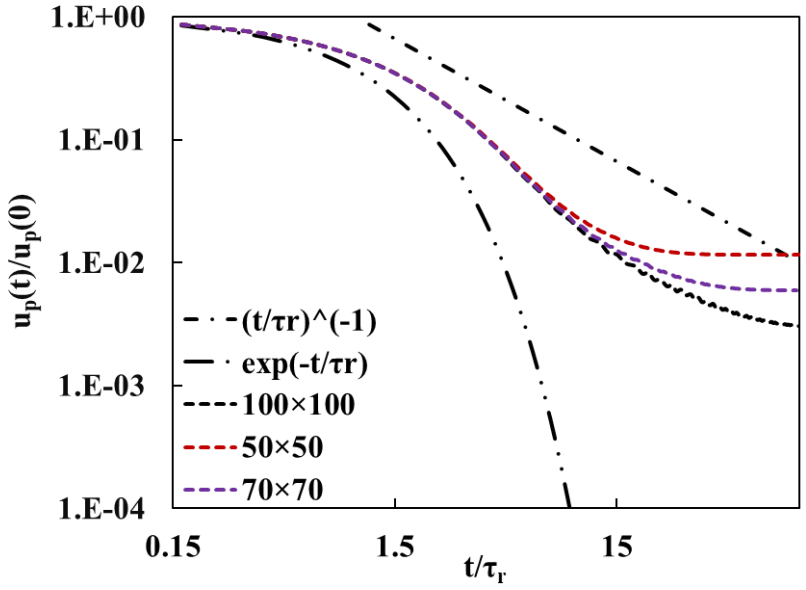

FIGURE 3 The momentum relaxation process of NP with different lattice Boltzmann fluid domains. The calculation domains are 100^2,70^2 and 50^2 with initial velocity of 0.01.

In order to characterize the momentum change process in the single relaxation process of the NP, the x and y axes are characterized by standardized time and velocity, where the x axis is the dimensionless relaxation time, which is defined as t/τ_r τ_r is the time scale parameter of the momentum relaxation of particles, and the y axis is the dimensionless velocity, which is defined as the ratio of the current velocity to the initial velocity. According to the research of Alder et al.[41], the momentum relaxation process of single particle conforms to the exponential decay law in the early stage, and then begins to enter the decay process of power function relationship. This decay relationship in the middle and late stages is called the long tail effect, which also reflects the fluid-particle coupling effect.

From Figure 3, the relaxation process of NPs is different under different computational domain conditions. Under the condition of small computational domain (50^2), the particle momentum decay is smaller, because in the case of small computational domain, the NPs relax to the equilibrium state by less viscous force. In this simulation, the early decay relationship of NPs in the three computational domains follows exponential decline, then the slope of the decay segment follows a power function relationship. Finally, the particles enter the equilibrium state with the same velocity as the fluid. Due to the different computational domains, the corresponding equilibrium velocity is negatively correlated with the size of the computational domain.

Example 2: Brownian motion in the dilute colloid system

Due to the collision of water molecules, NPs will generate irregular Brownian motion, which meets the fluctuation-dissipation theory. Previous studies[42,43] have shown that once the fluid phase satisfies the heat dissipation theory through fluctuation dynamics, particle dynamics will automatically satisfy the heat dissipation theory through the coupling of particle fluid. However, when considering the introduction of thermal fluctuations at the same time, it is necessary to rescale the mobility of particles to capture Brownian motion, and empirical scaling often lacks physical meaning[37]. Liu et al.[27] chose not to add thermal fluctuations in the fluid phase but only to add thermal fluctuations in the particle phase, directly capturing the Brownian motion of particles, avoiding the empirical scaling problem. In this case, the calculation formula of random force in the work of Liu et al.[27] was used to consider the Brownian motion of NPs in the dilute colloidal system, and the interaction force between NPs and NPs-microchannel surface was ignored. The influence of random force on NPs was only considered to simulate the motion process. In the dilute colloidal suspension system, the particle diameter of 10 nm, 50 nm, 100 nm, 1000 nm are simulated. The particle diffusion problem in the long time scale and the two dimensional diffusion coefficient in the long time scale can be calculated by the following formula.

where, $< >$represents the ensemble average of NPs, and D^{∞} represents the two-dimensional spatial diffusion coefficient. In order to avoid the interaction between particles, the initial simulation should ensure that the volume concentration of NPs is less than 0.1 %.

The Brownian diffusion coefficient of particles in a dilution boundaryless colloidal suspension system can be theoretically calculated by Stokes-Einstein relation

where, D^B is the theoretical solution of Brownian diffusion coefficient of particles, T is the absolute temperature, andζ is the friction coefficient.

Figure 4 shows the relationship between the mean square displacement of NPs and time. In the logarithmic coordinate system, the mean square displacement of NPs is basically linear with time, and the Brownian diffusion coefficient increases with the decrease of particle size, which reflects that under the small particle size, the relative impact level of water molecules on particles is more intense, and with the increase of particle size, the impact of water molecules on particles is relatively weak.

Figure 5 shows the correlation between the simulation results and the Stokes-Einstein relation curve. The simulation results are in good agreement with the theoretical solution, which proves that the method can

capture the Brownian motion of NPs.

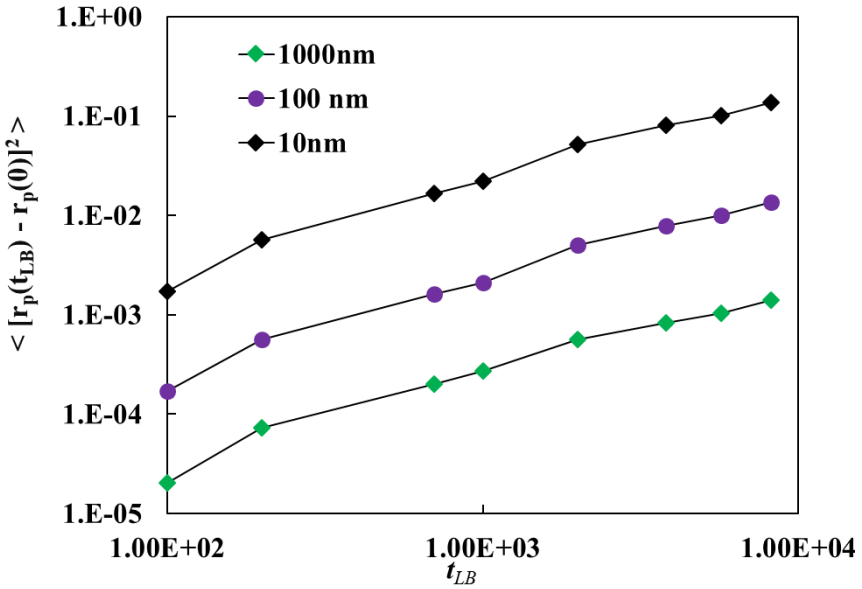

FIGURE 4 The relationship of mean squared displacements and time with various particle sizes

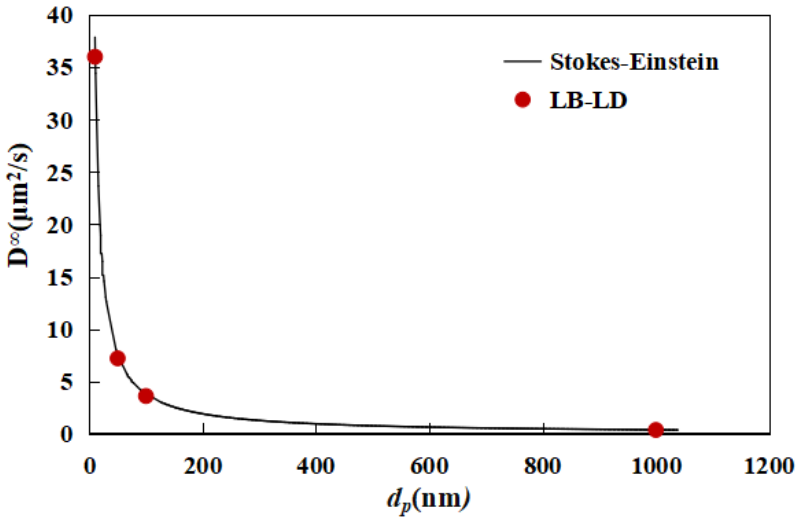

FIGURE 5 Comparison between theoretical and simulated results of Brownian diffusion coefficient

Example 3: The attachment efficiency of NPs onto channel surface

In the works of [14,44,45], two dimensionless parameters are used to characterize the electrostatic force. Given as

Where N_{E1} and N_{DL}represents the magnitudes of surface potentials and the ratio of NP radius to double layer thickness, respectively. $\varphi_1$andφ_2 are the surface potentials on the NP and microchannel surface, respectively.

In this work, φ_1 and φ_2 are both equal to -30 mV, and N_{E1} is 9; Reynold number equals to 1. The relationship of N_{DL} and attachment ratio of NPs is depicted in Figure 6. The attachment ratio of NPs is increased with the augment of N_{DL} .

By comparison, it is found that the current simulation results are in good results with the previous ones, which verifies the effectiveness of this developed LB-LD method. It not only verifies the correctness of the LBM used to simulate the flow field, but also verifies the correctness of the particle dynamics simulation, which lays the foundation for the following simulation of particle transport and attachment processes.

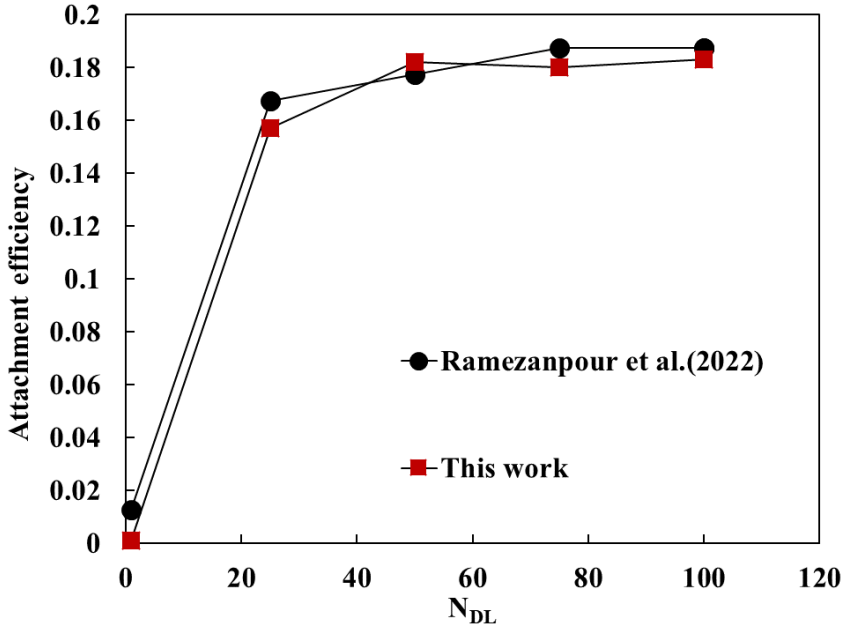

FIGURE 6 Attachment ratio of NPs in a microchannel versus N_{DL} with Re = 1, N_{E1}=10 and comparison with results of Ramezanpour et al.[14]

4 RESULTS AND DISCUSSION

4.1 The attachment of NPs in a microchannel

A variety of factors could affect the attachment of NPs over the transport process, at least including, NP diameter, Reynolds number, ionic strength, NP and microchannel surface potential. In this section, the impacts of all the above factors onto the attachment of NPs are investigated comprehensively.

In Figure 7, L is the length of the microchannel and H is the width of the microchannel. The inlet boundary condition is constant velocity boundary condition and the outlet is constant pressure condition. The L equals to 24 μm and H is 1.2 μm in the whole simulation. The other main physical parameters used in the simulation are showed in Table 1. The transport and attachment processes of NPs in a microchannel are showed in Figure 8. As a result of particle-wall interaction, particle-particle interaction and hydrodynamic effect, the transport behavior and attachment efficiency of NPs could be quite different.

TABLE 1 The range of physical parameters used in the simulation.

Parameters	Values
Particle diameter	5 – 25 nm
Reynold number, *Re*	0.1 – 10
Ionic strength (salt concentration)	0.001 – 0.1 M
Surface potential of NPs Surface potential of wall Temperature	-50 – -10 mV -20 mV 373 K

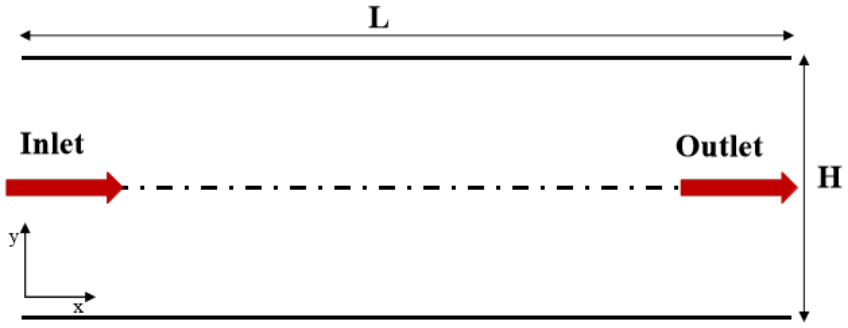

FIGURE 7 A schematic diagram of the geometry characteristic of the microchannel

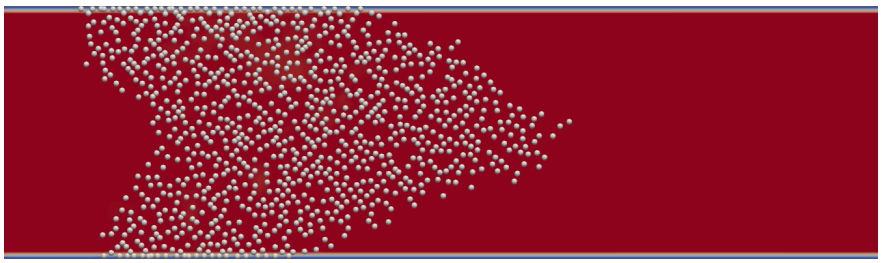

FIGURE 8 Transport and attachment processes of NPs. The NPs are injected randomly form the inlet of microchannel.

Figure 9 shows the relationship between NP diameter and attachment efficiency with different *Re* . The attachment efficiency is defined as the number of NPs attaching onto the microchannel over the total injection number of NPs. The attachment efficiency is negatively linearly correlated to the particle diameter. And the slopes of the three lines are degressive with enhanced Reynold number. Because the diffusion coefficient of smaller particle is higher as showed in Figure 5. The random Brownian motion plays an more important role in attachment process thus NPs have more probability of attachment to the microchannel surface. As the increases of *Re* (i.e., the hydrodynamic effect in Eq. 8 would be enhanced), the convection of NPs flow is more dominant than the diffusion, leading to the further dampened of attachment process. Therefore, the NP with strong Brownian diffusion and weak hydrodynamic effect is prone to have high attachment efficiency

Figure 10 shows the relationship between ionic strength (IS) and attachment efficiency with different *Re* . The ionic is assumed to 1:1 electrolyte NaCl. The zeta potentials of NPs in different IS are referred from[46-48].When the ionic strength is 0.001 M, NPs are hardly attached to the microchannel. While increase of the ionic strength leads to higher attachment efficiency. All these three lines show corresponding threshold value with the 0.01 M ionic strength. The reason for different ionic strength lays in the electrostatic force between NPs and the microchannel surface. When the ionic strength is lower (0.001 M), the interaction force between NPs and the microchannel surface shows repulsive characteristic since the electrostatic force

is more dominant than van der Waals force. Then the increase of ionic strength results in the compressed electric double layer and lower zeta potentials of NPs. Therefore, the interaction forces between NPs and the microchannel surface behave like attractive characteristic. When the ionic strength increases to 0.01 M, the van der Waals attractive force is much greater than the electrostatic force. The effect of van der Waals force on the attachment behavior of NPs could be dominant. Additionally, the increased *Re* will lead to lower attachment efficiency in the same ionic strength. This is also because the hydrodynamic damping effect.

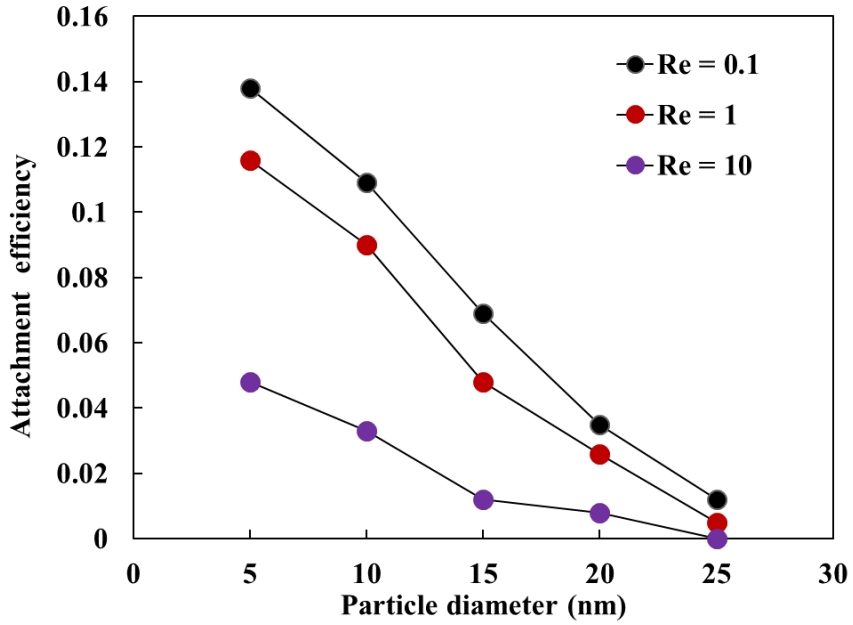

FIGURE 9 Attachment ratio of NPs versus diameter under different *Re* number. The ionic strength is 0.001 M and the surface potential of NPs is -50 mV.

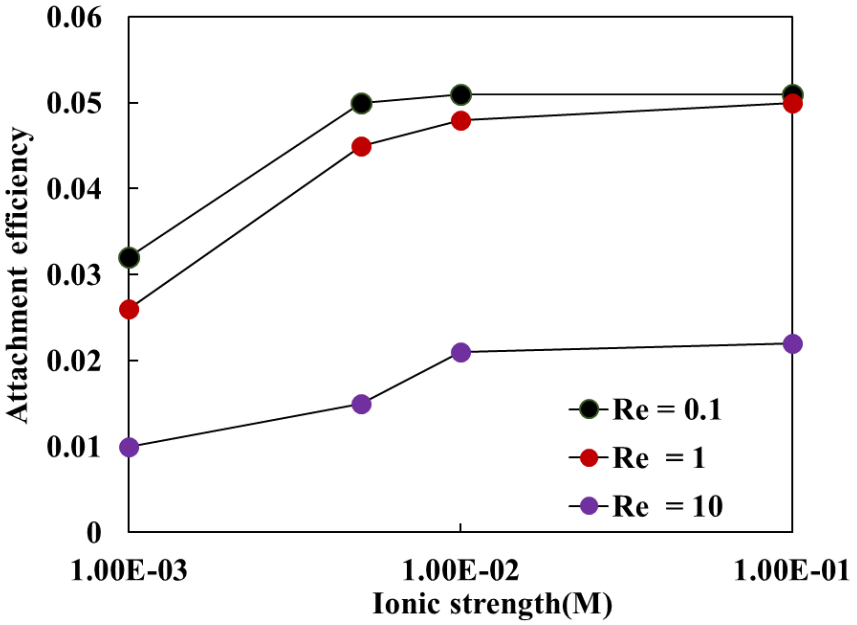

FIGURE 10 The effect of NP ionic strength on the NP attachment ratio for different values of Reynolds number. The diameter of NPs is 20 nm.

4.2 Flow pattern of NPs in the transport process

In this section, the effect of the interaction force influencing the NP flow pattern is investigated.

When investigating the NP attachment process, most models are ignoring the interaction force between NPs and collisions between NPs. While the interaction forces between NPs should not be omitted in dense colloid system. Therefore, this case adopts one-way coupled LB-LD method. The interaction forces affect the flow regime of NPs in bulk flow and diffusion of NPs. This model which considers the interaction forces could simulate the transport and attachment process of NPs more accurately.

The aggregation rate is represented by coordination number. The coordination number is defined as the contacts number of particle over the total primary particle number[21]. As exhibited in Figure 11, the aggregation rate is increased with the improvement of salt concentration. The coordination number of NPs are about 0.04, 0.5, 1.5, 8 with corresponding ionic strength of 0.001 M, 0.005 M, 0.01 M, 0.1 M. Figure 12 shows potential curve of NP-NP interaction in different ionic strength. The energy barrier decreases with the increase of ionic strength. According to the DLVO theory, the electric double layer is compressed with the increase of the ionic strength. Therefore, the electrostatic potential decreases and the interaction energy is dominant by van der Waals potential.

Figure 13 shows the distribution pattern of NPs in quiescent condition with different values of IS. It is clearly showed that the ordered pattern of particles in lower ionic strength (0.001 M) and clustered pattern in higher ionic strength (0.1 M). The intermedia range of IS (0.005 M and 0.01 M) shows a mixture of ordered and clustered NPs. Different distribution pattern could be interpreted by the DLVO theory. When the ionic strength is lower, the electrostatic potential energy greater than van der Waals potential energy. In other words, the electrostatic force is stronger than van der Waals force. The particles tend to repulsive to each other, resulted in better stability. While in high ionic strength (0.1 M) van der Waals attraction force dominates electrostatic repulsion and cause the NPs to aggregate.

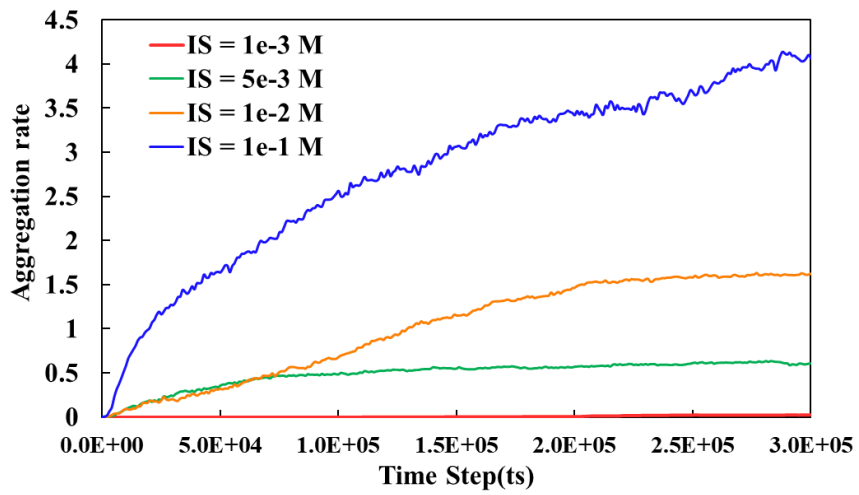

FIGURE 11 The aggregation rate of NPs with different values of ionic strength ‘

(Corresponding ionic strength is 0.001 M, 0.005 M, 0.01 M, 0.1 M with particle size of 20 nm. The aggregation rate is simulated in stationary state)

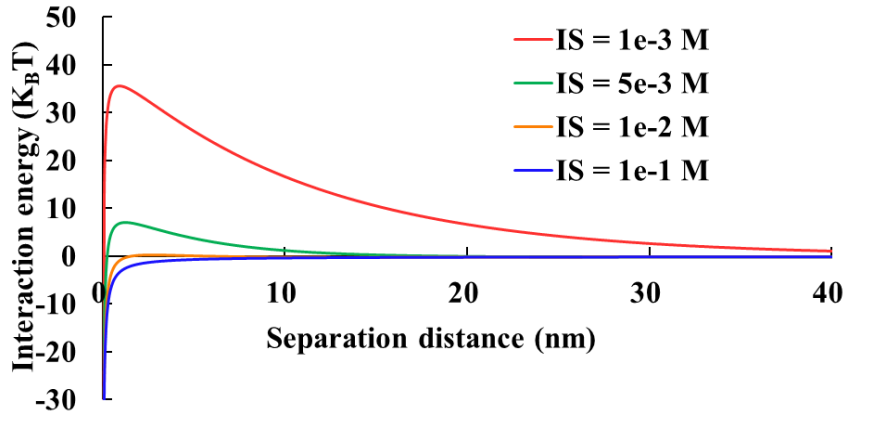

FIGURE 12 The potential curve of NP-NP interaction in different ionic strength. The ionic strength is 0.001 M, 0.005 M, 0.01 M, 0.1 M with particle size of 20 nm.

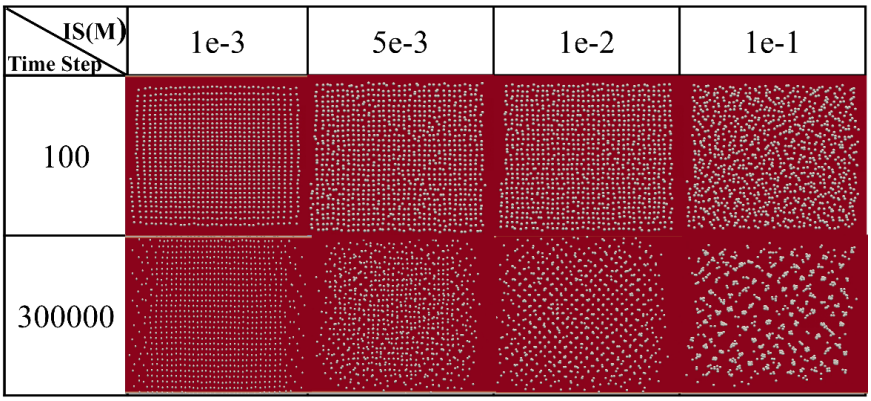

FIGURE 13 NPs distribution pattern with different values of ionic strength and NPs surface potential.

(Corresponding ionic strength is 0.001 M, 0.005 M, 0.01 M, 0.1 M with particle size of 20 nm.)

Table 2 shows the max coordination number used for classifying the different flow patterns in the transport process of NPs. The coordination number is an important factor to describe the aggregation structure. When the max coordination number is less than 0.1, the flow pattern of NPs is isolated regime. When the max coordination number is more than 1, the flow pattern of NPs is clustered regime. And when the max coordination number is between 0.1 and 1, the flow pattern of NPs is transitional regime.

A general phase diagram composed of three flow patterns considering hydrodynamic effect and DLVO theory is obtained in Figure 14. Compared with quiescent condition, when the ionic strength is strong (0.1 M), NPs present a clustered state, as the decrease of the ionic strength, the NP flow behaves like mixed structure. Finally, the NP depicts isolated regime as the magnitude of ionic strength is lower. The increased Re induces parabolic shape of flow patterns. The stronger hydrodynamic effect resulted in better dispersion. The general phase diagram is important for predicting the flow pattern of NPs in specified values of ionic strength and Re .

TABLE 2 Coordination number of NPs with different ionic strength and Re.

Re IS(M)	0	0.01	0.1	1
0.001	0.04	0.03	0.86	0.33
0.005	0.50	0.65	0.73	0.45
0.01	1.50	1.69	1.32	0.57
0.1	8.05	9.14	5.76	1.09

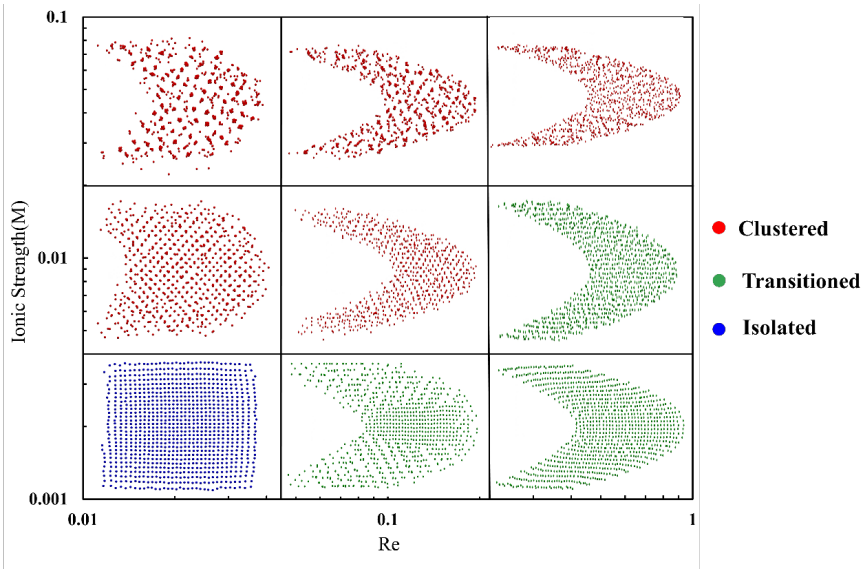

FIGURE 14 General phase diagram of NPs flow regime with different values of ionic strength and Re. (The diameter of NPs is 20 nm. The blue, green and red are representing isolated, mixed and clustered regime respectively. The aqueous phase is hid to see the flow pattern of NPs clearly.)

5 CONCLUSIONS

The transport and attachment processes of charged NPs are investigated by extending the two-way coupled LB-LD method[27,28]. Random force of NPs, friction force of NPs, van der Waals force and electrostatic force between NPs and the microchannel are considered in this Euler-Lagrange method. Moreover, this method considers the van der Waals force and double layer electrostatic force between NPs in order to simulate the transport and attachment process of NPs more accurately. The results provided valuable information on the underlying mechanisms of transport and attachment processes of NPs. 1 The attachment behavior of NPs is governed by DLVO theory, Brownian diffusion and hydrodynamic effect. The attachment efficiency is decreasing with the increasing nanoparticle diameter due to the diffusion coefficient is negatively correlated with the particle diameter. The increasing Reynolds number decreasing the attachment chance of NPs for the Hydrodynamic damping effect. 2 There exists a critical ionic strength for the attachment efficiency, beyond which the NPs do not attach to the microchannel because the van der Waals attractive force is much greater than the electrostatic force. The effect of van der Waals force on the attachment behavior of NPs could be dominant. 3 For relatively high ionic strength (more than 0.01 M), a clustered structure of nanoparticle suspensions is observed for the dominance of van der Waals force; whereas for relatively low ionic strength (less than 0.005 M), an ordered structure of nanoparticle suspensions is obtained due to the dominance of electrostatic repulsion force. 4 A general phase diagram including these flow patterns (isolated, transitional and clustered regime) is obtained for predicting the transport behavior of NPs with specified ionic strength and Reynolds number.

This coupled LB-LD method achieves the efficient-yet-rigorous characterization of NPs transport and attachment processes. Moreover, this method can be extended to investigate transport and attachment processes of NPs with multiphase flow in porous media in the future.

NOMENCLATURE

Acc	the Hamaker constant (J)
Cs	pseudo sound velocity (m s^{-1})
D_{ij}	the minimum distance between NP i and NP j
D^{∞}	the two-dimensional spatial diffusion coefficient (m^2 s^{-1})
D^{B}	the theoretical solution of Brownian diffusion coefficient of particles (m^2 s^{-1})
d_p	the diameter of NP (nm)
$\overrightarrow{E}_P^i$	the electrostatic force of NPs i (N)
$\overrightarrow{e}_i$	the unit vector of the particle velocity component
$\overrightarrow{F}_P^i$	the friction force of NPs i (N)
f_i	the particle distribution function in i direction
f_i^s	the distribution function of the force source term of the fluid in the direction i
f_i^{eq}	the distribution function of the equilibrium state
H	the width of the microchannel (μm)
I	characteristic tensor
L	the length of the microchannel (μm)
m_p^i	the mass of NP i (kg)
N	the total number of NPs
N_{E1}	the magnitudes of surface potentials
N_{DL}	the ratio of NP radius to double layer thickness
Q	discrete direction number
R	the radius of NP (nm)
r_a	the location of the fluid node (m)
$r_{p,a}$	the location of the center of the NPs (m)
$\overrightarrow{S}_P^i$	the random force of NPs (N)
T	the absolute temperature (K)
$\overrightarrow{u}$	fluid velocity (m s^{-1})
$\overrightarrow{u}_w(\overrightarrow{r_P}, t)$	the velocity of water at the corresponding position of particles (m s^{-1})
$\overrightarrow{V}_P^i$,	the van der Waals force between NPs (N)
Z	the interaction constant
z	the electrolyte valence
Greek symbols	
ε_0	the vacuum dielectric constant, ε_0 = 8.85*1e-12 F/m
ε	the relative dielectric constant of water, ε = 78.5
κ	reciprocal of Debye length (m^{-1})
τ	single relaxation time
φ_1	the surface potential of NP (V)
φ_2	the surface potential of microchannel (V)
ζ	the friction coefficient
μ_w	the dynamic viscosity of the aqueous phase (mPa·s)
ψ	the shape coefficient of the NPs
ω_i	weight coefficient in i direction
$?_{\mathrm{ij}}$	Kronecker deltas

Acc	the Hamaker constant (J)
$?_{??}$	Kronecker deltas
Subscripts	
w	Water phase
p	nanoparticle

ACKNOWLEDGEMENTS

The authors would like to acknowledge financial support provided by National Natural Science Foundation of China (No. 52074338). We are also grateful to the support of the National Key R&D Program of China (No. 2019YFA0708700), and National Key Basic Research Program of China (20CX06071A). Bin Yuan would like to thank for the support of Shandong Mountain Tai Scholar Program.

REFERENCE

1. Khan I, Saeed K, Khan I. Nanoparticles: Properties, applications and toxicities. *Arabian Journal of Chemistry.*2019;12(7):908-931.

2. Guo D, Xie G, Luo J. Mechanical properties of nanoparticles: basics and applications. *Journal of Physics D: Applied Physics.*2014;47(1).

3. verma Sk, Tiwari AK. Application of Nanoparticles in Solar collectors: A Review. *Materials Today: Proceedings.* 2015/01/01/ 2015;2(4-5):3638-3647.

4. Mitchell MJ, Billingsley MM, Haley RM, Wechsler ME, Peppas NA, Langer R. Engineering precision nanoparticles for drug delivery.*Nature Reviews Drug Discovery.* 2021/02/01 2021;20(2):101-124.

5. Mohan Bhagyaraj S, Oluwafemi OS. Nanotechnology: The Science of the Invisible. In: Mohan Bhagyaraj S, Oluwafemi OS, Kalarikkal N, Thomas S, eds. *Synthesis of Inorganic Nanomaterials* : Woodhead Publishing; 2018:1-18.

6. Kot M, Major Ł, Lackner JM, Chronowska-Przywara K, Janusz M, Rakowski W. Mechanical and Tribological Properties of Carbon-Based Graded Coatings. *Journal of Nanomaterials.* 2016/02/10 2016;2016:1-14.

7. Zhe Z, Yuxiu A. Nanotechnology for the oil and gas industry – an overview of recent progress. *Nanotechnology Reviews.*2018;7(4):341-353.

8. William JKM, Ponmani S, Samuel R, Nagarajan R, Sangwai JS. Effect of CuO and ZnO nanofluids in xanthan gum on thermal, electrical and high pressure rheology of water-based drilling fluids. *Journal of Petroleum Science and Engineering.* 2014/05/01/ 2014;117:15-27.

9. Agista M, Guo K, Yu Z. A State-of-the-Art Review of Nanoparticles Application in Petroleum with a Focus on Enhanced Oil Recovery. *Applied Sciences.* 2018;8(6).

10. Feder J. Random sequential adsorption. *Journal of Theoretical Biology.* 1980/11/21/ 1980;87(2):237-254.

11. Kubala P, Batys P, Barbasz J, Weronski P, Ciesla M. Random sequential adsorption: An efficient tool for investigating the deposition of macromolecules and colloidal particles. *Adv Colloid Interface Sci.* Aug 2022;306:102692.

12. Mahian O, Kolsi L, Amani M, et al. Recent advances in modeling and simulation of nanofluid flows-Part I: Fundamentals and theory. *Physics Reports.* 2019;790:1-48.

13. Mahian O, Kolsi L, Amani M, et al. Recent advances in modeling and simulation of nanofluid flows—Part II: Applications.*Physics Reports.* 2019;791:1-59.

14. Ramezanpour M, Siavashi M, Raeini AQ, Blunt MJ. Pore-scale simulation of nanoparticle transport and deposition in a microchannel using a Lagrangian approach. *Journal of Molecular Liquids.*2022;355.

15. Kasbaoui MH, Koch DL, Desjardins O. Clustering in Euler–Euler and Euler–Lagrange simulations of unbounded homogeneous particle-laden shear. *Journal of Fluid Mechanics.*2018;859:174-203.

16. Chou Y-J, Gu S-H, Shao Y-C. An Euler–Lagrange model for simulating fine particle suspension in liquid flows. *Journal of Computational Physics.* 2015;299:955-973.

17. Capecelatro J, Desjardins O. An Euler–Lagrange strategy for simulating particle-laden flows. *Journal of Computational Physics.* 2013;238:1-31.

18. Bahiraei M. Studying nanoparticle distribution in nanofluids considering the effective factors on particle migration and determination of phenomenological constants by Eulerian–Lagrangian simulation. *Advanced Powder Technology.* 2015;26(3):802-810.

19. Aminfar H, Mohammadpourfard M, Mortezazadeh R. Numerical simulations of the influence of Brownian and gravitational forces on the stability of CuO nanoparticles by the Eulerian-Lagrangian approach.*Heat Transfer-Asian Research.* 2018;47(1):72-87.

20. Liu H, Lu J, Liu D, Cui F. Brownian Dynamic Study of the Aggregation Process of TiO2 Nanoparticles in Aqueous Suspensions.*Environmental Engineering Science.* 2018;35(9):996-1004.

21. Peng Z, Doroodchi E, Evans G. DEM simulation of aggregation of suspended nanoparticles. *Powder Technology.*2010;204(1):91-102.

22. Liu HH, Surawanvijit S, Rallo R, Orkoulas G, Cohen Y. Analysis of nanoparticle agglomeration in aqueous suspensions via constant-number Monte Carlo simulation. *Environ Sci Technol.* Nov 1 2011;45(21):9284-9292.

23. Samari-Kermani M, Jafari S, Rahnama M, Raoof A. Ionic strength and zeta potential effects on colloid transport and retention processes. *Colloid and Interface Science Communications.* 2021;42.

24. Murray CA, Grier DG. Video Microscopy of Monodisperse Colloidal Systems. *Annual Review of Physical Chemistry.*1996;47(1):421-462.

25. Srivastava S, Nykypanchuk D, Fukuto M, et al. Two-dimensional DNA-programmable assembly of nanoparticles at liquid interfaces. *J Am Chem Soc.* Jun 11 2014;136(23):8323-8332.

26. Kelley JJ, Jespersen ML, Vaia RA. Self-limiting gold nanoparticle surface assemblies through modulation of pH and ionic strength. *Journal of Nanoparticle Research.* 2018;20(11):1-13.

27. Liu Z, Zhu Y, Clausen JR, Lechman JB, Rao RR, Aidun CK. Multiscale method based on coupled lattice-Boltzmann and Langevin-dynamics for direct simulation of nanoscale particle/polymer suspensions in complex flows. *International Journal for Numerical Methods in Fluids.* 2019;91(5):228-246.

28. Liu Z, Zhu Y, Rao RR, Clausen JR, Aidun CK. Nanoparticle transport in cellular blood flow. *Computers & Fluids.*2018;172:609-620.

29. Liu Z, Clausen JR, Rao RR, Aidun CK. Nanoparticle diffusion in sheared cellular blood flow. *Journal of Fluid Mechanics.*2019;871:636-667.

30. Shiyi C, Doolen. GD. LATTICE BOLTZMANN METHOD FOR FLUID FLOWS. *Annual Review of Fluid Mechanics.* 1998;31(1):329-364.

31. Aidun CK, Clausen JR. Lattice-Boltzmann Method for Complex Flows. *Annual Review of Fluid Mechanics.* 2010 2010;42(1):439-472.

32. Israelachvili J. *Intermolecular and Surface Forces* . Oxford: Elsevier; 2011.

33. Bhatnagar PL, Gross EP, Krook M. A Model for Collision Processes in Gases. I. Small Amplitude Processes in Charged and Neutral One-Component Systems. *Physical Review.* 05/01/ 1954;94(3):511-525.

34. Yun BM, Dasi LP, Aidun CK, Yoganathan AP. Highly resolved pulsatile flows through prosthetic heart valves using the entropic lattice-Boltzmann method. *Journal of Fluid Mechanics.* Sep 2014;754:122-160.

35. Di Ilio G, Dorschner B, Bella G, Succi S, Karlin IV. Simulation of turbulent flows with the entropic multirelaxation time lattice Boltzmann method on body-fitted meshes. *Journal of Fluid Mechanics.* Jun 15 2018;849:35-56.

36. D'Humieres D, Ginzburg I, Krafczyk M, Lallemand P, Luo LS. Multiple-relaxation-time lattice Boltzmann models in three dimensions.*Philos Trans A Math Phys Eng Sci.* Mar 15 2002;360(1792):437-451.

37. Ahlrichs P, Dünweg B. Lattice-Boltzmann Simulation of Polymer-Solvent Systems. *International Journal of Modern Physics C.* 2011;09(08):1429-1438.

38. Peskin CS. The immersed boundary method. *Acta Numerica.* 2003;11:479-517.

39. He X, Zou Q, Luo L-S, Dembo M. Analytic solutions of simple flows and analysis of nonslip boundary conditions for the lattice Boltzmann BGK model. *Journal of Statistical Physics.* 1997/04/01 1997;87(1-2):115-136.

40. d'Humières DJPTotRSoLSAM, Physical, Sciences E. Multiple–relaxation–time lattice Boltzmann models in three dimensions. 2002;360(1792):437-451.

41. Alder BJ, Wainwright TE. Decay of the Velocity Autocorrelation Function. *Physical Review A.* 01/01/ 1970;1(1):18-21.

42. Mazur P. On the motion and Brownian motion of n spheres in a viscous fluid. *Physica A: Statistical Mechanics and its Applications.* 1982/01/01/ 1982;110(1-2):128-146.

43. Hauge EH, Martin-Löf A. Fluctuating hydrodynamics and Brownian motion. *Journal of Statistical Physics.* 1973/03/01 1973;7(3):259-281.

44. Rajagopalan R, Kim JS. Adsorption of brownian particles in the presence of potential barriers: effect of different modes of double-layer interaction. *Journal of Colloid and Interface Science.* 1981/10/01/ 1981;83(2):428-448.

45. Seetha N, Majid Hassanizadeh S, Mohan Kumar MS, Raoof A. Correlation equations for average deposition rate coefficients of nanoparticles in a cylindrical pore. *Water Resources Research.*2015;51(10):8034-8059.

46. Dong S, Zeng Z, Cai W, et al. The zeta potentials of g-C3N4 nanoparticles: Effect of electrolyte, ionic strength, pH, and humic acid. *Journal of Nanoparticle Research.* 2019;21(11):1-12.

47. Yang F, Wu W, Chen S, Gan W. The ionic strength dependent zeta potential at the surface of hexadecane droplets in water and the corresponding interfacial adsorption of surfactants. *Soft Matter.*Jan 18 2017;13(3):638-646.

48. Irigoyen J, Arekalyan VB, Navoyan Z, Iturri J, Moya SE, Donath E. Spherical polyelectrolyte brushes' constant zeta potential with varying ionic strength: an electrophoretic study using a hairy layer approach. *Soft Matter.* 2013;9(48):11609-11617.